

# Internal Boundary Control of Lane-Free Automated Vehicle Traffic using a Model-Free Adaptive Controller

Milad Malekzadeh, Ioannis Papamichail, Markos Papageorgiou

*Dynamic Systems and Simulation Laboratory, Technical University of Crete, Chania 73100, Greece  
(e-mails: mmalek@dssl.tuc.gr; ipapa@dssl.tuc.gr; markos@dssl.tuc.gr)*

**Abstract:** In lane-free traffic, recently proposed for connected automated vehicles (CAV), incremental changes of the road width lead to corresponding incremental changes of the traffic flow capacity. This property enables the controlled shifting of the internal road boundary separating the two opposite traffic directions, so as to optimize the road infrastructure utilization. Internal boundary control aims at flexible sharing of the total road width and capacity among the two traffic directions of a road in real-time-, in response to the prevailing traffic conditions. A model-free adaptive control scheme is applied to efficiently address this problem. Simulation investigations, involving a realistic highway stretch and challenging demand scenario, demonstrate that the efficiency of the proposed control scheme.

**Keywords:** lane-free traffic, internal boundary control, model-free adaptive control, capacity sharing.

## 1. INTRODUCTION

Recurrent traffic congestion is an increasingly serious problem for big cities around the world. It is causing substantial delays, increased fuel consumption, excessive environmental pollution and reduced traffic safety. Conventional traffic management measures are valuable (Papageorgiou et al., 2003; Kurzhanskiy and Varaiya, 2010) and, in some cases, able to delay or even avoid the onset of congestion. However, they are not always sufficient to tackle heavily congested traffic conditions. Vehicle Automation and Communication Systems (VACS) should be exploited to develop innovative solutions that can be applied within a smart road infrastructure. During the last decade, there has been an enormous effort by the industry and by many research institutions to develop and deploy a variety of VACS that are revolutionizing the vehicle capabilities and may be exploited for improved traffic management (Diakaki et al., 2015).

The TrafficFluid concept was recently launched by Papageorgiou et al. (2021). This is a novel paradigm for vehicular traffic in the era of high penetration rates of vehicles equipped with highly advanced VACS. The TrafficFluid concept suggests: (1) lane-free traffic, whereby vehicles are not bound to fixed traffic lanes, as in conventional traffic; (2) vehicle nudging, whereby vehicles may exert a "nudging" effect on, i.e. influence the movement of, other vehicles in front of them. In this context, the internal boundary control concept, introduced by Malekzadeh et al. (2021), exploits the lane-free principle of TrafficFluid. In lane-free traffic, the road capacity may exhibit incremental (increasing or decreasing) changes in response to corresponding incremental (widening or narrowing) changes of the road width. This is in contrast to lane-based traffic, where capacity changes may only occur if the road width is changed by one or more lanes.

Consider a road with two opposite traffic directions serving connected automated vehicles (CAVs). The total available cross-road capacity (for both directions) may be shared among the two directions in a flexible way, according to the prevailing demand per direction. Flexible capacity sharing may be achieved by virtually moving the internal boundary that separates the two traffic directions; and communicating this decision to CAVs, so that they respect the changed road boundary. This way, the total capacity share assigned per direction can be changed in space and time according to an appropriate real-time control strategy, as illustrated in Fig. 1, so as to maximize the traffic efficiency of the overall system.

The idea of sharing the total cross-road capacity among the two traffic directions is not new as it has been occasionally employed for conventional lane-based traffic, typically with manual interventions (Wolshon and Lambert, 2006). The measure is known as tidal flow (or reversible lanes) control and its main principle is to adapt the total available supply to the demand per direction. Its most basic form is the steady allocation of one or more lanes of one direction to the other direction for a period of time, so as to address abnormal traffic supply or demand. More advanced reversible lane control systems may operate in real time, e.g. to balance delays on both sides of a known bottleneck (e.g. bridge, tunnel) by assigning a lane to one of the two directions in alternation in response to the prevailing traffic conditions. In order to deal with this problem, optimal control or feedback control algo-

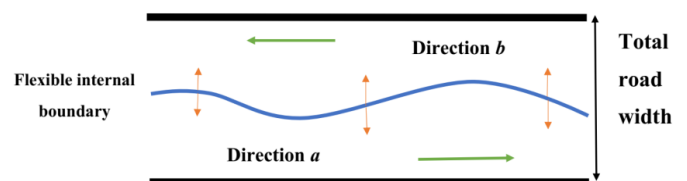


Fig. 1: Space-time flexible internal road boundary

gorithms of various types were proposed by Frejo et al. (2015) and Ampountolas et al. (2020). Reversible lanes have also been considered in connection with lane-based CAV driving (see e.g. work by Duell et al. (2015) and Levin and Boyles (2016)),

The use of tidal flow control systems in lane-based traffic is not widespread for a number of reasons, including the harsh resolution of infrastructure sharing (only by lane quanta) among the two traffic directions; the serious counter-problems due to frequent merging or diverging traffic at lane-drop or lane-gain areas; and the long safety-induced time-delays after each lane switch. These serious difficulties entail very limited capacity sharing flexibility in space and time and hinder reversible lane control from being a major traffic management measure. Even in the future CAV traffic, some of the mentioned difficulties would persist in lane-based conditions, notably the low capacity sharing resolution and the merging nuisance. In contrast, in a lane-free CAV traffic environment, the mentioned difficulties are largely mitigated. More specifically, the resolution of road-width sharing among the two directions can be high, since the smooth CAV driving on a lane-free road surface allows for the internal boundary to be a smooth space-function, as illustrated in Fig. 1. Also, assuming moderate changes of the internal boundary over time and space, the aforementioned safety-induced time-delay may be very small.

Thanks to these characteristics, real-time internal boundary control for lane-free CAV traffic may be broadly applicable to the high number of arterial or highway infrastructures that feature unbalanced demands during the day in the two traffic directions, so as to strongly mitigate or even utterly avoid congestion. Malekzadeh et al. (2021) analyzed the internal boundary control problem and demonstrated its high improvement potential by formulating and solving an open-loop optimal control problem, in the form of a convex Quadratic Programming (QP) problem. That approach may be used within an MPC (Model Predictive Control) frame for real-time application, but simpler real-time approaches, which rely on real-time measurements and do not call for external demand prediction, but have nevertheless similar efficiency, are preferable. This paper explores the application of a recently proposed Model-Free Adaptive Control (MFAC) method for the internal boundary control problem.

MFAC methods have been given a lot of attention in the past 20 years and have been applied successfully in many different fields (see Hou and Wang, 2013; Hou et al., 2017 for an overview). An MFAC approach, initially developed for a class of Single-Input Single Output (SISO) nonlinear systems, was extended for a class of Multi-Input Multi-Output (MIMO) systems (see Hou and Jin 2011a; 2011b and references therein). Instead of identifying the nonlinear model of the process, local dynamic linearization data models are built while operating the closed-loop system utilizing a dynamic linearization method. Considering different memory requirements, three different dynamic linearization methods can be used. These are the compact form dynamic linearization, the partial form dynamic linearization and the full form dynamic linearization (Hou and Jin, 2014). It is interesting to note that,

recently, MFAC has been used within predictive control (Li et al., 2019) and iterative learning control (Ren et al., 2020) frameworks for perimeter control of urban road traffic networks.

Section 2 presents some background issues of internal boundary control, while Section 3 presents the appropriately adjusted Cell Transmission Model (CTM), initially proposed by Daganzo (1994), which is employed for simulation purposes. Section 4 presents the MFAC method applied. Simulation investigations are discussed in Section 5, where the performance of the MFAC is compared to the no-control case, while conclusions are given in Section 6.

## 2. BACKGROUND

Lane-free traffic is not expected to give rise to structural changes of existing macroscopic traffic flow models. As also supported by findings in (Bhavathrathan and Mallikarjuna, 2012; Asaithambi et al., 2016; Munigety et al., 2016; Papageorgiou et al., 2021), notions and concepts like the conservation equation, the Fundamental Diagram (FD), as well as moving traffic waves continue to characterize macroscopic traffic flow modelling in the case of lane-free CAV traffic. Additionally, specific physical traffic parameters, such as free speed, critical density, flow capacity, jam density, are also relevant for lane-free traffic, but may of course take different values than in lane-based traffic.

Let us call the two opposite traffic directions, presented in Fig. 1, directions  $a$  and  $b$ , respectively. We assume that, at specific road sections, each direction is assigned a respective road width  $w^a = \varepsilon \cdot w$  and  $w^b = (1 - \varepsilon) \cdot w$ , where  $w$  is the total road width (both directions) and  $0 \leq \varepsilon \leq 1$  is the sharing factor, which is specified in real time as a control input by the internal boundary controller.

Let  $Q(\rho)$ , where  $\rho$  is the traffic density in veh/km, be the FD of a road section, which would apply if the whole road width would be assigned to only one of the two opposite traffic directions (i.e. for  $\varepsilon$  equal 0 or 1), with total critical density  $\rho_{cr}$ , total capacity  $q_{cap}$  (in veh/h) and total jam density  $\rho_{max}$ . In the case of partial road sharing, we have  $\varepsilon_{min} \leq \varepsilon \leq \varepsilon_{max}$ , where  $\varepsilon_{min}, \varepsilon_{max} \in (0, 1)$  are appropriate bounds aiming to suppress utter closure of either direction. As shown by Malekzadeh et al. (2021), the FDs for the two directions are functions of  $\varepsilon$  given by

$$\begin{aligned} Q^a(\rho^a, \varepsilon) &= \varepsilon \cdot Q(\rho^a / \varepsilon) \\ Q^b(\rho^b, \varepsilon) &= (1 - \varepsilon) \cdot Q(\rho^b / (1 - \varepsilon)) \end{aligned} \quad (1)$$

where  $\rho^a$  and  $\rho^b$  (in veh/km) are the respective densities of the two directions.

For simulation purposes, a dynamic traffic flow model must be used. A simple, yet realistic, option is CTM (Daganzo, 1994), a first-order dynamic traffic flow model with a triangular FD, which attains a space-time discretized form by application of the Godunov numerical scheme. The following paragraphs present the CTM equations, appropriately adjusted to incorporate the effect of the sharing factor  $\varepsilon$ .

A highway stretch with two reverse traffic directions  $a$  (from left to right) and  $b$  (from right to left) is considered. The stretch is subdivided in  $n$  sections, with lengths  $L_i$ ,  $i=1,2,\dots,n$ . As explained above, the total road width, which is assumed constant over all sections for simplicity, can be flexibly shared among the two directions in real time. As the sharing may be different for every section, we have corresponding sharing factors  $\varepsilon_i$ ,  $i=1,2,\dots,n$ ; and (1) applies to each section. As a consequence, the total section capacity, as well as the critical density and jam density, are shared among traffic directions  $a$  and  $b$  according to

$$\begin{aligned} q_{i,cap}^a(\varepsilon_i) &= \varepsilon_i \cdot q_{cap}, & q_{i,cap}^b(\varepsilon_i) &= (1-\varepsilon_i) \cdot q_{cap} \\ \rho_{i,cr}^a(\varepsilon_i) &= \varepsilon_i \cdot \rho_{cr}, & \rho_{i,cr}^b(\varepsilon_i) &= (1-\varepsilon_i) \cdot \rho_{cr} \\ \rho_{i,max}^a(\varepsilon_i) &= \varepsilon_i \cdot \rho_{max}, & \rho_{i,max}^b(\varepsilon_i) &= (1-\varepsilon_i) \cdot \rho_{max}. \end{aligned} \quad (2)$$

The above derivations rely on the assumption, partially verified by Papageorgiou et al. (2021), that any incremental widening (narrowing) of the road width entails a corresponding incremental increase (decrease) of capacity. Indeed, the highway may hold vehicles of different dimensions and speeds. These vehicles spread, in a lane-free road structure, on the road surface according to their two-dimensional movement strategies, which lead to a variety of lateral vehicle positions, including vehicles driving on the road boundary (without ever exceeding it). Thus, every incremental widening of the road increases the average two-dimensional inter-vehicle spacing and offers possibilities for higher speed, and hence higher flow and capacity.

The corresponding changes of the triangular FD that occur at each section and traffic direction are illustrated in Fig. 2. More specifically, when the value of the sharing factor is 0.5, i.e., the flow capacities of the two directions are equal, their FDs are "nominal" (blue line with  $\cdot^N$  parameters); when the sharing factor is different than 0.5, we have two FDs: the extended one (green line with  $\cdot^E$  parameters) applies to the direction that is assigned more width and hence more flow capacity, and the reduced, complementary FD (orange line with  $\cdot^R$  parameters) applies to the other direction that is assigned less width and flow capacity. Based on (2), all FD parameters of a section change, whenever it is decided to change the corresponding sharing factor in real time.

While controlling the internal road boundary, we disallow the utter closure of either direction; hence, the assigned road width in either direction should not be smaller than the widest vehicles driving on the road. This requirement gives rise to stricter constraints for the sharing factors as follows

$$0 < \varepsilon_{i,min} \leq \varepsilon_i \leq \varepsilon_{i,max} < 1, \quad (3)$$

where  $\varepsilon_{i,min} \cdot w$  and  $(1-\varepsilon_{i,max}) \cdot w$  are the minimum admissible widths to be assigned to directions  $a$  and  $b$ , respectively.

Another restriction to be applied to the sharing factors concerns the time-delay needed to evacuate traffic on the direction that receives a restricted width, compared with the previous control time-step. This time-delay is small in lane-free CAV traffic with moderate changes of the sharing factors

applied to short sections. This time-delay is omitted here for simplicity but is considered in ongoing work. More generally, work in progress, involving micro-simulation of the internal boundary control concept, indicates that vehicles have no difficulty to adapt to the real-time change of the internal boundary, and no safety-critical situations have been observed.

### 3. SIMULATION MODEL

Traffic flows from section 1 to section  $n$  in direction  $a$ ; and from section  $n$  to section 1 in direction  $b$  (see Fig. 3 as an example). We denote  $\rho_i^a$ ,  $i=1,2,\dots,n$ , the traffic density of section  $i$ , direction  $a$ ; and  $\rho_i^b$ ,  $i=1,2,\dots,n$ , the traffic density of section  $i$ , direction  $b$ . Similarly, we denote  $q_i^a$ ,  $i=1,2,\dots,n$ , and  $q_i^b$ ,  $i=1,2,\dots,n$ , the mainstream exit flows of section  $i$  for directions  $a$  and  $b$ , respectively. Thus,  $q_0^a$  is the feeding upstream mainstream inflow for direction  $a$ ; and  $q_{n+1}^b$  is the feeding upstream mainstream inflow for direction  $b$ . Every section may have an on-ramp or an off-ramp at its upstream boundary. The on-ramp flows (if any) at section  $i$  are denoted  $r_i^a$  for direction  $a$ , and  $r_i^b$  for direction  $b$ . The off-ramp flow (if any) of section  $i$ , direction  $a$ , is calculated based on known exit rates  $\beta_i^a$  multiplied with the upstream-section flow, i.e.  $\beta_i^a q_{i-1}^a$ ; and the off-ramp flow (if any) of section  $i$ , direction  $b$ , is calculated based on known exit rates  $\beta_i^b$  multiplied with the upstream-section flow, i.e.  $\beta_i^b q_{i+1}^b$ .

The conservation equation for the section  $i$  of direction  $a$  is:

$$\rho_i^a(k+1) = \rho_i^a(k) + \frac{T}{L_i} ((1-\beta_i^a)q_{i-1}^a(k) - q_i^a(k) + r_i^a(k)), \quad (4)$$

where  $T$  is the model time-step, typically equal to 5 – 10 s for section lengths of some 500 m in length, and  $k=0,1,\dots$  is the discrete time index of the model.

According to CTM, traffic flow is obtained as the minimum of demand and supply functions, except for the very last sections, where only the demand function is considered, assuming that the downstream traffic conditions are uncongested. Clearly, the demand and supply functions  $Q_D$  and  $Q_S$ , respectively, for the case of the internal boundary control problem, include the impact of the respective sharing factors  $\varepsilon_i(k)$  on the sections' FDs. Thus we have

$$\begin{aligned} q_i^a(k) &= \min \left\{ Q_D(\rho_i^a(k), \varepsilon_i(k)), \frac{Q_S(\rho_{i+1}^a(k), \varepsilon_{i+1}(k))}{(1-\beta_{i+1}^a)} - r_{i+1}^a(k) \right\}, \\ & \quad i = 1, 2, \dots, n-1 \\ q_n^a(k) &= Q_D(\rho_n^a(k), \varepsilon_n(k)). \end{aligned} \quad (5)$$

The demand and supply functions are given by the following respective equations

$$\begin{aligned} Q_D(\rho, \varepsilon) &= \min \{ \varepsilon q_{cap}, v_f \rho \}, \\ Q_S(\rho, \varepsilon) &= \min \{ \varepsilon q_{cap}, w_s (\varepsilon \rho_{max} - \rho) \}, \end{aligned} \quad (6)$$

where  $v_f$  is the free speed (which is assumed equal for all sections for simplicity) and  $w_s$  is the back-wave speed.

The equations for section  $i$  of direction  $b$  are analogous to those of direction  $a$ , with few necessary index modifications. Section numbers in direction  $b$  are descending, hence we have

$$\rho_i^b(k+1) = \rho_i^b(k) + \frac{T}{L_i}((1-\beta_i^b)q_{i+1}^b(k) - q_i^b(k) + r_i^b(k)), \quad (7)$$

and the flows are given by

$$\begin{aligned} q_1^b(k) &= Q_D(\rho_1^b(k), (1-\varepsilon_1(k))) \\ q_i^b(k) &= \min\left\{Q_D(\rho_i^b(k), (1-\varepsilon_i(k))), \right. \\ &\quad \left. \frac{Q_S(\rho_{i-1}^b(k), (1-\varepsilon_{i-1}(k)))}{(1-\beta_{i-1}^b)} - r_{i-1}^b(k)\right\}, i = 2, 3, \dots, n \end{aligned} \quad (8)$$

## 4. MODEL-FREE ADAPTIVE CONTROLLER

### 4.1 Relative Densities

In conventional traffic management, traffic densities reflect the state of traffic. However, in the novel internal boundary control context, the variables  $\rho_i^a$  and  $\rho_i^b$  of the traffic densities (in veh/km) in the two opposite directions of each section  $i$  are not directly indicating the traffic conditions (e.g. under-critical or congested) encountered. This is because the critical density for each direction is changing according to the applied control action. Therefore, we define the *relative densities*  $\tilde{\rho}_i^a$  and  $\tilde{\rho}_i^b$  (dimensionless) that are given per section and per direction as the ordinary densities. The relative density of section  $i$  and direction  $a$  or  $b$  is obtained by dividing the corresponding traffic density with the corresponding critical density, which, on its term, depends on the sharing factor prevailing during the last time-step. Considering (2), we get the following relations for section  $i$

$$\tilde{\rho}_i^a(k) = \frac{\rho_i^a(k)}{\varepsilon_i(k-1)\rho_{cr}}, \quad \tilde{\rho}_i^b(k) = \frac{\rho_i^b(k)}{(1-\varepsilon_i(k-1))\rho_{cr}}. \quad (9)$$

### 4.2 Dynamic Linearization

In order to derive the MFAC scheme, we need to come up with a dynamic linearization model that describes our system.

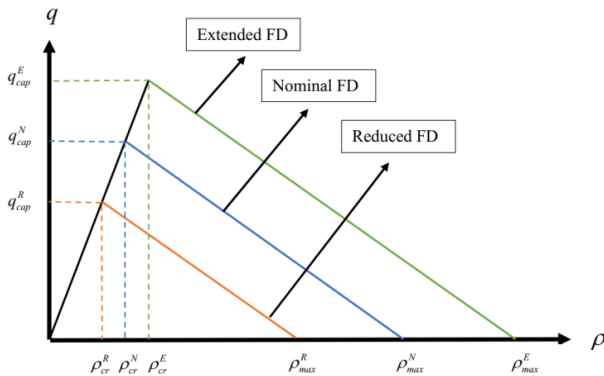


Fig. 2: The triangular fundamental diagram with flexible internal boundary

The following general form of a multi-input multi-output nonlinear discrete-time system is first considered

$$\mathbf{y}(k_c + 1) = \mathbf{f}(\mathbf{y}(k_c), \dots, \mathbf{y}(k_c - n_y), \mathbf{u}(k_c), \dots, \mathbf{u}(k_c - n_u)) \quad (10)$$

where  $\mathbf{y}(k_c) \in \mathbb{R}^p$  and  $\mathbf{u}(k_c) \in \mathbb{R}^p$  are the system outputs and inputs, respectively, and  $k_c$  is the discrete control time index.  $n_y$  and  $n_u$  are unknown orders,  $p$  is a known integer and  $\mathbf{f} \in \mathbb{R}^p$  is an unknown nonlinear function that describes the dynamics of the system.

For the internal boundary control problem, we will consider as an output the difference between the relative densities per direction for each section; and as an input the sharing factor for each section. Thus, we have  $\mathbf{y}(k_c) = \tilde{\boldsymbol{\rho}}^a(k_c) - \tilde{\boldsymbol{\rho}}^b(k_c)$  and  $\mathbf{u}(k_c) = \boldsymbol{\varepsilon}(k_c)$  with the integer  $p$  set equal to  $n$ , whereby  $\tilde{\boldsymbol{\rho}}^a(k_c) = [\tilde{\rho}_1^a(k_c), \dots, \tilde{\rho}_n^a(k_c)]^T$ ,  $\tilde{\boldsymbol{\rho}}^b(k_c) = [\tilde{\rho}_1^b(k_c), \dots, \tilde{\rho}_n^b(k_c)]^T$  and  $\boldsymbol{\varepsilon}(k_c) = [\varepsilon_1(k_c), \dots, \varepsilon_n(k_c)]^T$ .

Note that the control time-step is assume to be a multiple of the simulation model time-step, i.e.  $T_c = MT$ , where  $M$  is an integer. As a result, the discrete control time index is  $k_c = \lfloor kT/T_c \rfloor$ , where  $\lfloor \cdot \rfloor$  is the integer part notation.

According to Hou and Jin (2011b), the compact-form dynamic linearization of the nonlinear system (10) is based on the following assumptions.

*Assumption 1:* The partial derivatives of  $\mathbf{f}$  with respect to the control inputs  $\mathbf{u}(k_c)$  are continuous.

*Assumption 2:* System (10) is generalized Lipschitz, i.e.  $\|\Delta\mathbf{y}(k_c + 1)\| \leq b\|\Delta\mathbf{u}(k_c)\|$  for each fixed  $k_c$  and  $\|\Delta\mathbf{u}(k_c)\| \neq 0$ , where  $b$  is a positive constant,  $\Delta\mathbf{y}(k_c + 1) = \mathbf{y}(k_c + 1) - \mathbf{y}(k_c)$  and  $\Delta\mathbf{u}(k_c) = \mathbf{u}(k_c) - \mathbf{u}(k_c - 1)$ .

Both assumptions are reasonable from a practical point of view. Assumption 1 is a typical condition, while assumption 2 limits the rate of changes of the system outputs when changes are applied to the control inputs. Based on the above, it can be shown that there must exist a non-unique  $p \times p$  matrix  $\boldsymbol{\Phi}(k_c)$ , called Pseudo-Partial Derivative (PPD), such that (10) can be transformed into the following equivalent compact-form dynamic linearization data model:

$$\Delta\mathbf{y}(k_c + 1) = \boldsymbol{\Phi}(k_c)\Delta\mathbf{u}(k_c) \quad (11)$$

where  $\|\boldsymbol{\Phi}(k_c)\| \leq b$ . The matrix  $\boldsymbol{\Phi}(k_c)$  is regarded to be a slowly time-varying parameter.

Compared to several other linearization methods (e.g. Taylor's linearization, feedback linearization, orthogonal function approximation), the compact-form dynamic linearization is based only on the input-output data of the controlled process, i.e. no model dynamics are needed. Model (11) is simple, and the dynamically changing PPD matrix can be easily estimated using data collected from the closed-loop system.

### 4.2 Controller Design

According to Hou and Jin (2011b), another assumption is necessary:

*Assumption 3:* The PPD matrix  $\Phi(k_c)$  is a diagonally dominant matrix in the following sense,  $|\phi_{ij}| \leq b_1$ ,  $b_2 \leq |\phi_{ii}| \leq ab_2$ ,  $i=1, \dots, p$ ,  $j=1, \dots, p$ ,  $i \neq j$ ,  $a \geq 1$ ,  $b_2 > b_1(2a+1)(p-1)$ , and the sign of all the elements of  $\Phi(k_c)$  is not changing.

We now consider the following objective function:

$$J = \|\mathbf{y}^*(k_c+1) - \mathbf{y}(k_c+1)\|^2 + \lambda \|\mathbf{u}(k_c) - \mathbf{u}(k_c-1)\|^2 \quad (12)$$

where  $\mathbf{y}^*(k_c+1)$  is the desired output and  $\lambda > 0$  is a weighting constant. The MFAC scheme, suggested by Hou and Jin (2011b), is as follows:

$$\mathbf{u}(k_c) = \mathbf{u}(k_c-1) + \frac{\nu \hat{\Phi}^T(k_c)(\mathbf{y}^*(k_c+1) - \mathbf{y}(k_c))}{\lambda + \|\hat{\Phi}(k_c)\|^2} \quad (13)$$

where  $\nu \in (0, 1]$  is a step-size constant used for stability purposes. The unknown PPD matrix is estimated using the modified projection algorithm via

$$\hat{\Phi}(k_c) = \hat{\Phi}(k_c-1) + \frac{\eta(\Delta \mathbf{y}(k_c) - \hat{\Phi}(k_c-1)\Delta \mathbf{u}(k_c-1))\Delta \mathbf{u}^T(k_c-1)}{\mu + \|\Delta \mathbf{u}(k_c-1)\|^2} \quad (14)$$

where  $\eta \in (0, 2]$  is a step-size constant and  $\mu > 0$  is a weighting factor. The outcome of (14) is reset, whenever Assumption 3 does not hold true, using the following rules:

$$\begin{aligned} \hat{\phi}_{ii}(k_c) &= \hat{\phi}_{ii}(1), & \text{if } |\hat{\phi}_{ii}(k_c)| < b_2 \text{ or } |\hat{\phi}_{ii}(k_c)| > ab_2 \\ & & \text{or } \text{sign}(\hat{\phi}_{ii}(k_c)) \neq \text{sign}(\hat{\phi}_{ii}(1)) \\ \hat{\phi}_{ij}(k_c) &= \hat{\phi}_{ij}(1), & \text{if } |\hat{\phi}_{ij}(k_c)| > b_1 \text{ or } \text{sign}(\hat{\phi}_{ij}(k_c)) \\ & & \neq \text{sign}(\hat{\phi}_{ij}(1)), i \neq j \end{aligned} \quad (15)$$

where  $\hat{\phi}_{ij}(1)$   $i=1, \dots, p$ ,  $j=1, \dots, p$ , is the initial value for each element of the PPD matrix, which has been selected so that Assumption 3 holds true.

It can be shown (see Theorem 3 by Hou and Jin (2011b)) that if the nonlinear system (10), satisfying Assumptions 1, 2 and 3, is controlled by the MFAC scheme (13)-(15) for  $\mathbf{y}^*(k_c+1) = \mathbf{y}^*$ , i.e. a constant set-point, then there exists a  $\lambda_{\min} \geq 0$ , for which the selection of  $\lambda > \lambda_{\min}$  guarantees that:

1.  $\lim_{k_c \rightarrow \infty} \|\mathbf{y}^*(k_c+1) - \mathbf{y}^*\| = 0$  monotonically; and
2.  $\{\mathbf{y}(k_c)\}$  and  $\{\mathbf{u}(k_c)\}$  are bounded sequences.

For the internal boundary control problem, the application of the above scheme, with a set point  $\mathbf{y}^* = \mathbf{0}$ , will tend towards a state where, for every section, the relative densities per direction are equal to each other. Striving for the same value of the relative densities on the two directions at each section seems equitable; and is also conforming with the operational objective of balancing the margin to capacity across sections. Finally, the use of the second term in (12) penalizes possible oscillations of the sharing factor over time.

For practical implementation, the values obtained for each control variable are truncated before application in order to

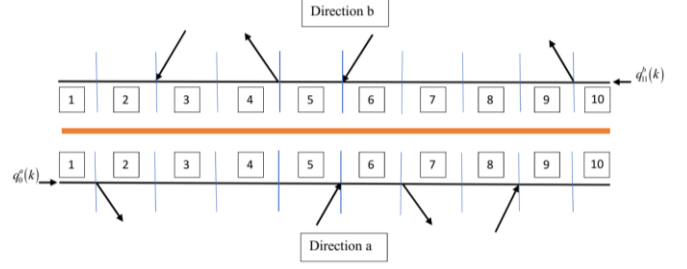


Fig. 3: The considered highway stretch

satisfy (3). These truncated values are used as  $\mathbf{u}(k_c-1)$  in (13) in the next time step.

## 5. SIMULATION INVESTIGATIONS

### 5.1 Simulation Set-up

The performance of the proposed model-free adaptive control scheme is investigated using the bi-directional highway stretch depicted in Fig. 3. The considered highway stretch has a length of 5 km and is subdivided in 10 sections of 0.5 km each. The modelling time-step,  $T$ , is set to 10 s, and the considered time horizon is 1 h, so 360 model time-steps are simulated. CTM is used as the emulated ground truth. The model parameters used are  $v_f = 100$  km/h and  $w_s = 12$  km/h; while the total cross-road capacity to be shared among the two directions is  $q_{cap} = 12,000$  veh/h. The exit rates for the four off-ramps are all equal to 0.1.

The mainstream and on-ramp demand flows per direction are presented in Fig. 4. It may be seen that the two directions feature respective peaks in their mainstream demands that are slightly overlapping. The on-ramp demands are constant and are all equal to 1000 veh/h. The simulation results of the no-control case are presented first, followed by the results obtained when using the MFAC scheme.

### 5.2 No-control Case

Using the demand flows presented above in the CTM equations with constant sharing factors  $\varepsilon_i = 0.5$  for all sections due to no internal boundary control, we obtain the simulation

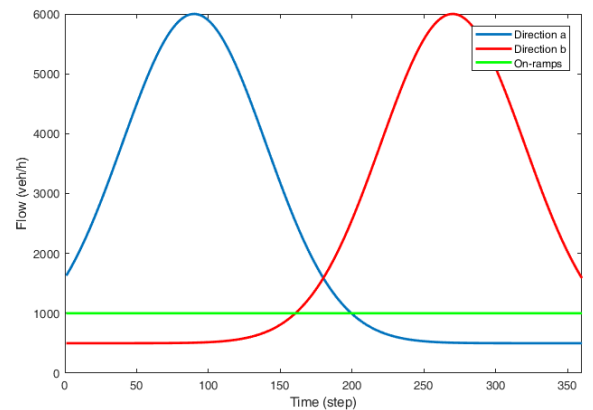


Fig. 4: Demand flows per direction and on-ramp

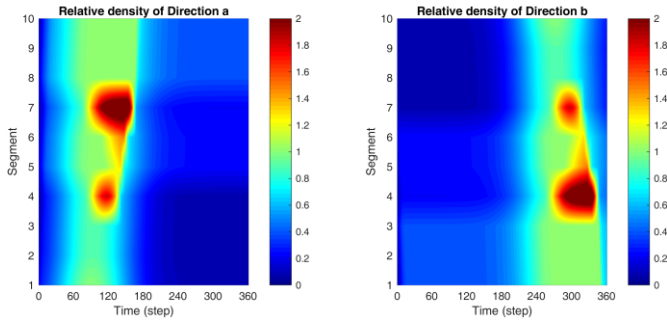


Fig. 5: Relative density for the two directions in the no-control case

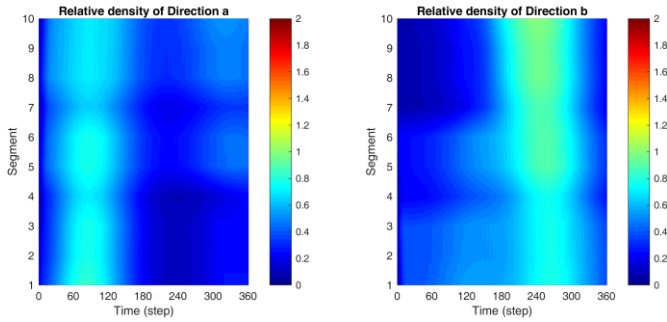


Fig. 6: Relative density for the two directions in the control case

results of the no-control case with a TTS (Total Time Spent by all vehicles in the highway stretch) value equal to 314.6 veh-h. Fig. 5 displays the corresponding spatio-temporal evolution of the relative density defined in (9). According to the definition, relative density values lower than 1 refer to uncongested traffic; while values higher than 1 refer to congested traffic; when the relative density equals 1, and the downstream section is uncongested, we have capacity flow at the corresponding section.

Fig. 5 shows that congestion is created in sections 5 and 8 for direction  $a$  due to the increased mainstream demand, in combination with the ramp inflows, at around  $k = 60$ . The congestion dissolves at around  $k = 160$ , due to the rapid decrease of the mainstream demand for this direction. In direction  $b$ , we have also congestion being triggered in sections 3 and 6 for similar reasons, at around  $k = 240$ . The congestion dissolves at around  $k = 340$ .

### 5.3 Control Case

The MFAC scheme starts with initial control input values set equal to the nominal values, i.e. equal to 0.5 for all sections, while the control time-step,  $T_c$ , is set to 60 s. The following values that satisfy Assumption 3 are selected for initialization and bounding of the elements of the PPD matrix  $\Phi(k_c)$ :  $\alpha = 2$ ,  $b_1 = 0.05$ ,  $b_2 = 2.25$ ,  $\phi_{ii}(1) = -3.375$  and  $\phi_{ij}(1) = -\phi_{ji}(1) = -0.05$ ,  $i = 1, \dots, 10$ ,  $j = 1, \dots, 10$ ,  $i < j$ . The controller parameters are selected after some tuning to be:  $\nu = 0.5$ ,  $\lambda = 30$ ,  $\eta = 1$  and  $\mu = 0.1$ . Finally, the upper and lower bounds for the sharing factors, used to avoid blocking

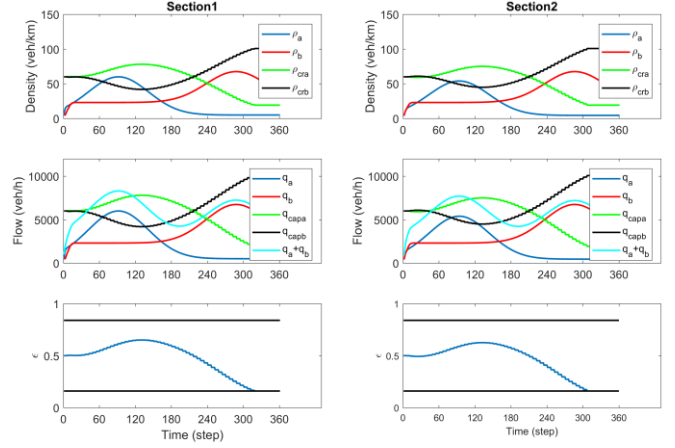


Fig. 7: Density, flow and control trajectories in the control case (sections 1 and 2)

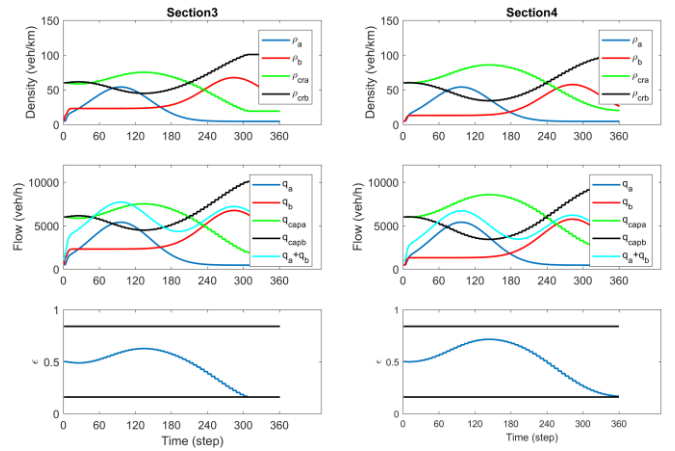


Fig. 8: Density, flow and control trajectories in the control case (sections 3 and 4)

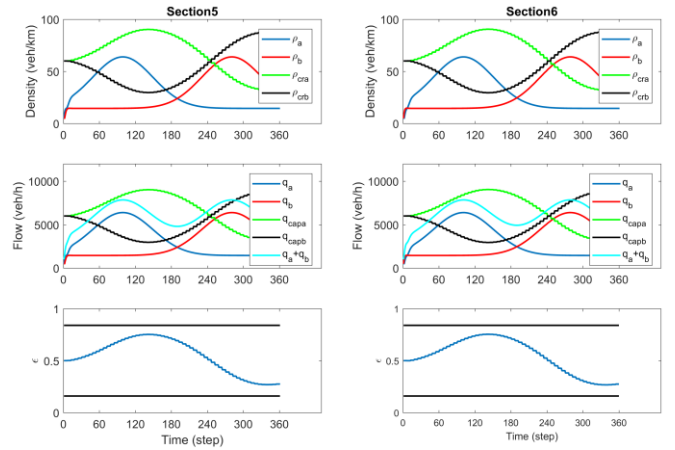


Fig. 9: Density, flow and control trajectories in the control case (sections 5 and 6)

of any of the two directions, are equal for all sections  $i = 1, 2, \dots, 10$  and are given the values  $\varepsilon_{i,\min} = 0.16$  and  $\varepsilon_{i,\max} = 0.84$ .

With these settings, the regulator is operated in a closed-loop mode, receiving in emulated real time all section density val-

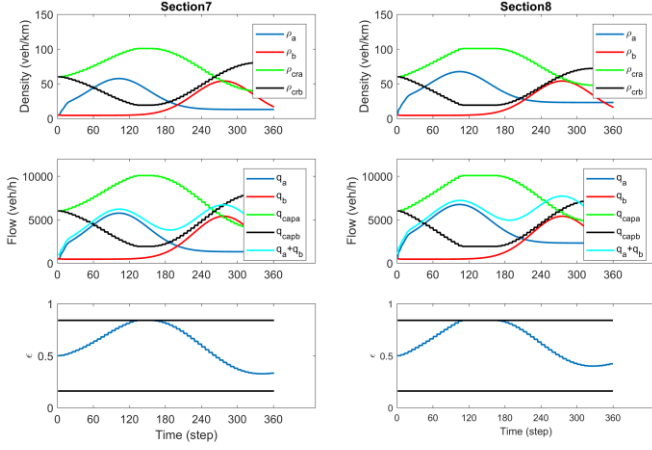


Fig. 10: Density, flow and control trajectories in the control case (sections 7 and 8)

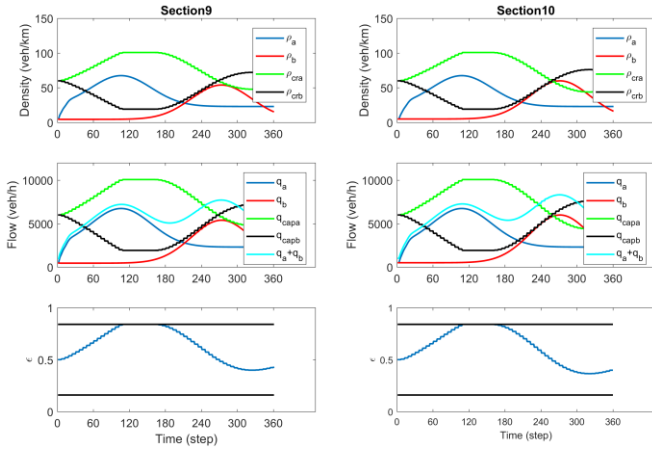


Fig. 11: Density, flow and control trajectories in the control case (sections 9 and 10)

ues per direction from the CTM equations; and responding with the sharing factors calculated using (13).

The resulting traffic conditions are under-critical everywhere as shown in the spatio-temporal evolution of the relative densities depicted in Fig. 6. More detailed information for this case is presented in Figs. 7-11. Each figure has two columns reflecting the results of two respective sections; for each section (column), we provide three diagrams (rows):

- The first diagram shows the two traffic densities (in veh/km), for directions  $a$  and  $b$ , and the corresponding critical densities, which are changing according to the sharing factor in the section.
- The second diagram shows the two traffic flows, for directions  $a$  and  $b$ , and the corresponding capacities, which are changing according to the sharing factor in the section. In addition, the sum of both flows is also displayed (cyan curve).
- The third diagram shows the value of the control input, i.e. the sharing factor applied, as well as the constant bounds (black curves), which may lead to possible truncation of the control input.

The displayed results confirm that densities (flows) are always lower than the respective critical densities (capacities) in all sections and in both directions; hence traffic conditions are always and everywhere under-critical. In fact, the total-flow curve (for both directions) does not reach the total road capacity (of 12,000 veh/h) at any time anywhere. In short, congestion is utterly avoided and any occurring delays in the no-control case do not exist anymore.

The sharing factor trajectories of the sections reveal that this outcome is enabled via a smooth swapping of assigned capacity to the two directions, whereby more capacity is assigned to direction  $a$  during the first half of the time horizon and more capacity is assigned to direction  $b$  during the second half, in response to the traffic density changes caused by the changing respective demands and their peaks. However, the sharing achieved is not completely balanced. This is possibly due to the initial values used for the elements of the PPD matrix. Though this sharing is not really harmful for the specific scenario, as congestion on either direction is utterly avoided, the sharing behaviour will need to be looked upon carefully in other demand or infrastructure scenarios in ongoing work.

The related TTS value is 288.9 veh·h, indicating an improvement of 8.2% over the no-control case. The TTS value obtained using the MFAC scheme is, in fact, equal to the value that is achieved when applying the optimal control resulting from the QP problem formulation presented by Malekzadeh et al. (2021). Thus, despite its simple feedback character, where no demand predictions are used, the model-free regulator achieves the highest possible efficiency in the investigated scenario.

## 6. CONCLUSIONS

The concept of internal boundary control, introduced by Malekzadeh et al. (2021), has been addressed in this study by use of a different control approach. A model-free adaptive controller was employed and preliminarily tested in a simulated environment involving a challenging traffic demand scenario. The well-known CTM, appropriately modified to introduce the effect of the sharing factors, has been used for simulation purposes.

In internal boundary control, the total road width and capacity are shared in each section in real time among the two directions of the road in response to the prevailing traffic conditions. The model-free regulator was found to be easy to design and implement (feedback-based) and robust to disturbances (no need to predict the arriving demands) for the tested scenario. More specifically, simulation investigations, using a challenging traffic demand scenario, demonstrated that the model-free regulator is equally efficient as an open-loop optimal control solution (with perfect demand prediction) developed for the same problem by Malekzadeh et al. (2021) on the basis of a convex QP problem formulation. The usefulness of the proposed control approach needs to be consolidated in future work via consideration of further challenging demand scenarios, as well as more realistic large-scale highway infrastructures, leading to different traffic conditions and decisions for the internal boundary control problem in lane-free traffic.

Other ongoing work considers the development of model-based control approaches (e.g. Linear Quadratic Regulators). Furthermore, microscopic simulation studies with vehicles moving in a lane-free mode, based on appropriate CAV movement strategies is currently under development.

#### ACKNOWLEDGMENTS

The research leading to these results has received funding from the European Research Council under the European Union's H2020 Programme / ERC Grant Agr. no. 833915, project TrafficFluid, see: <https://www.trafficfluid.tuc.gr>.

#### REFERENCES

- Ampountolas, K., dos Santos, J.A. and Carlson, R.C. (2020). Motorway tidal flow lane control. *IEEE Transactions on Intelligent Transportation Systems*, 21(4), 1687-1696.
- Asaithambi, G., Kanagaraj, V. and Toledo, T. (2016). Driving behaviors: Models and challenges for non-lane based mixed traffic. *Transportation in Developing Economies*, 2, no 19.
- Bhavathrathan, B. and Mallikarjuna, C. (2012). Evolution of macroscopic models for modeling the heterogeneous traffic: an Indian perspective. *Transportation Letters*, 4(1), 29-39.
- Daganzo, C.F. (1994). The cell transmission model: A dynamic representation of highway traffic consistent with the hydrodynamic theory. *Transportation Research Part B: Methodological*, 28(4), 269-287.
- Diakaki, C., Papageorgiou, M., Papamichail, I. and Nikolos I. (2015). Overview and analysis of vehicle automation and communication systems from a motorway traffic management perspective. *Transportation Research Part A: Policy and Practice*, 75, 147-165.
- Duell, M., Levin, M.W., Boyles, S.D. and Waller, S.T., (2015). System optimal dynamic lane reversal for autonomous vehicles, *2015 IEEE 18th International Conference on Intelligent Transportation Systems*, 1825-1830.
- Frejo, J.R.D., Papamichail, I., Papageorgiou, M. and Camacho, E.F. (2015). Macroscopic modeling and control of reversible lanes on freeways. *IEEE Transactions on Intelligent Transportation Systems*, 17(4), 948-959.
- Hou, Z. and Jin, S. (2011a). A novel data-driven control approach for a class of discrete-time nonlinear systems. *IEEE Transactions on Control Systems Technology*, 19(6), 1549-1558.
- Hou, Z. and Jin, S. (2011b). Data-driven model-free adaptive control for a class of MIMO nonlinear discrete-time systems. *IEEE Transactions on Neural Networks*, 22(12), 2173-2188.
- Hou, Z.S., Chi, R.H., Gao, H.J. (2017). An overview of dynamic linearization based data-driven control and applications. *IEEE Transactions on Industrial Electronics*. 64(5), 4076-4090.
- Hou, Z.S., Jin, S.T. (2014). *Model Free Adaptive Control: Theory and Applications*. CRC Press, Taylor and Francis Group, Florida.
- Hou, Z.S., Wang, Z. (2013). From model-based control to data-driven control: Survey, classification and perspective. *Information Science*, 235, 3-35.
- Kurzhanskiy, A.A. and Varaiya, P. (2010). Active traffic management on road networks: a macroscopic approach. *Philosophical Transactions of the Royal Society A: Mathematical, Physical and Engineering Sciences*, 368(1928), 4607-4626.
- Levin, M.W. and Boyles, S.D. (2016). A cell transmission model for dynamic lane reversal with autonomous vehicles. *Transportation Research Part C: Emerging Technologies*, 68, 126-143.
- Li, Z., Jin, S., Xu, C. and Li, J. (2019). Model-free adaptive predictive control for an urban road traffic network via perimeter control. *IEEE Access*, 7, 172489-172495.
- Malekzadeh, M., Papamichail, I., Papageorgiou, M. and Bogenberger, K. (2021). Optimal internal boundary control of lane-free automated vehicle traffic, *Transportation Research Part C*, 126, 103060.
- Munigety, C.R. and Mathew, T.V. (2016). Towards behavioral modeling of drivers in mixed traffic conditions. *Transportation in Developing Economies*, 2, no 6.
- Papageorgiou, M., Diakaki, C., Dinopoulou, V., Kotsialos, A. and Wang, Y. (2003). Review of road traffic control strategies. *Proceedings of the IEEE*, 91(12), 2043-2067.
- Papageorgiou, M., Mountakis, K.S., Karafyllis, I., Papamichail, I. and Wang Y. (2021). Lane-free artificial-fluid concept for vehicular traffic. *Proceeding of the IEEE*, 109, 114-121.
- Ren, Y., Hou, Z., Sirmatel, I.I. and Geroliminis, N. (2020). Data driven model free adaptive iterative learning perimeter control for large-scale urban road networks. *Transportation Research Part C: Emerging Technologies*, 115, 102618.
- Wolshon, B. and Lambert, L. (2006). Reversible lane systems: Synthesis of practice. *Journal of Transportation Engineering*, 132(12), 933-944.